

Complexity of Gaussian boson sampling with tensor networks

Minzhao Liu,^{1,2} Changhun Oh,³ Junyu Liu,^{3,4,5,6,7,8} Liang Jiang,^{3,5} and Yuri Alexeev^{2,4,5}

¹*Department of Physics, The University of Chicago, Chicago, IL 60637, USA*

²*Computational Science Division, Argonne National Laboratory, Lemont, IL 60439, USA*

³*Pritzker School of Molecular Engineering, The University of Chicago, Chicago, IL 60637, USA*

⁴*Department of Computer Science, The University of Chicago, Chicago, IL 60637, USA*

⁵*Chicago Quantum Exchange, Chicago, IL 60637, USA*

⁶*Kadanoff Center for Theoretical Physics, The University of Chicago, Chicago, IL 60637, USA*

⁷*qBraid Co., Chicago, IL 60615, USA*

⁸*SeQure, Chicago, IL 60615, USA*

Gaussian boson sampling, a computational model that is widely believed to admit quantum supremacy, has already been experimentally demonstrated to surpass the classical simulation capabilities of even the most powerful supercomputers today. However, whether the current approach limited by photon loss and noise in such experiments prescribes a scalable path to quantum advantage is an open question. For example, random circuit sampling with constant noise per gate was recently shown not to be a scalable approach to achieve quantum supremacy, although simulating intermediate-scale circuits is still very difficult. To understand the effect of photon loss on the scalability of Gaussian boson sampling, we use a tensor network algorithm with $U(1)$ symmetry to examine the asymptotic operator entanglement entropy scaling, which relates to the simulation complexity. We developed a custom-built algorithm that significantly reduces the computational time with state-of-the-art hardware accelerators, enabling simulations of much larger systems. With this capability, we observe, for Gaussian boson sampling, the crucial $N_{\text{out}} \propto \sqrt{N}$ scaling of the number of surviving photons in the number of input photons that marks the boundary between efficient and inefficient classical simulation. We further theoretically show that this result generally holds for other input states.

I. INTRODUCTION

Quantum mechanical systems are interesting because of superposition, where particles can occupy multiple states simultaneously, leading to exotic behaviors and novel phenomena that cannot be understood classically. To fully represent quantum systems classically, resources that scale exponentially with system sizes are necessary, and exact classical simulations are intractable. As a result, computations using quantum systems have been proposed to achieve improvement in algorithmic complexities in tasks such as integer factoring [1], unstructured search [2], linear algebra [3], Hamiltonian simulations [4–7], and more [8]. Present-day quantum computational devices, however, are susceptible to noise and cannot be perfectly controlled. As a result, numerous approaches based on sampling outputs of randomly configured devices have been proposed to demonstrate quantum supremacy, which are especially appealing considering near-term constraints. For example, recent

experimental efforts to demonstrate quantum supremacy using boson sampling [9–27], a process of sampling the photon output patterns from interferometers which is especially friendly to implementation with present-day linear optical devices, has inspired a plethora of subsequent works. Especially notable are works focusing on improving the hardness of simulation under realistic experimental restrictions [26–31], and proposals to exploit the scheme for practical problems [32–35]. For example, it is known that the input photon state to the interferometer affects the simulation hardness [36], and light sources with quantum properties are necessary for quantum advantage. Early experiments use single photons as a source of quantumness, but the probabilistic nature of heralded approaches of single-photon generation renders this approach unscalable. Numerous approaches have been proposed to improve the scalability of the photon source while maintaining the hardness of the problem [29–31]. The most promising approach is gaussian boson sampling (GBS), where no post-selection is necessary and classical simulation is hard unless some plausible complexity-theoretic conjectures are false [37, 38]. This allowed recent experimental demonstrations of GBS to claim quantum supremacy [26, 27].

In addition to innovations to the photon source, efforts to improve the simulation hardness of the experiments are also cognizant of the fact that boson sampling with realistic photon loss, unlike their idealized lossless counterparts, may be efficiently simulable using approximate schemes [39–42]. As a result, proposed schemes of improvement generally avoid high-depth optical circuits while trying to maintain high connectivity between optical modes [27, 28]. Although carving out a small regime under which approximate sampling is hard to simulate, these schemes limit the experiments, potential algorithms that can be performed, and most importantly, the complexity [43, 44]. Additional investigations are necessary for understanding the effect of loss on the asymptotic complexity of proposed quantum algorithms for scalable quantum supremacy demonstration.

The effects of noise are already examined in various contexts of quantum computing experiments. For qubits cases, it has long been known that without error correction, a quantum state after a large depth with a constant level of depolarizing noise becomes very close to the maximally mixed state [45], which enables an efficient approximate simulation. Therefore, for quantum supremacy demonstrations with noisy random circuit sampling (RCS) [46], where measurement output bit-strings

of a randomly chosen quantum circuit are sampled, the hope is to find an appropriate scale of experiments that is not too large to lose the quantum signal but not too small to be classically tractable. In a similar manner, it was numerically shown that the density operator entanglement entropy (EE), which relates to the complexity of the classical simulation, decreases if the circuit depth is too high for 1D [47] and 2D [48] systems. Further, the maximum achievable EE follows area law scaling, suggesting the possibility of efficient tensor network simulation. More recently, polynomial time simulation of RCS with constant depolarizing noise per gate is proven to be possible in an asymptotic regime for a depth larger than logarithmic scaling, denying the scalability of RCS, although not practically applicable to current RCS experiments due to a large degree of polynomials [49].

Meanwhile, in the context of boson sampling, a similar study has very recently shown that for a particular noise, which may not be experimentally relevant, there is an efficient classical algorithm for noisy boson sampling in an asymptotic regime [50]. Thus, the experimental noise might prohibit scalable quantum advantage in boson sampling, much like in RCS. However, it still remains possible for noisy boson sampling to be scalable under realistic noises, such as photon loss [39–42] and partial distinguishability [41, 51–54]. Notably, for photon loss, there have been many studies on its effect on the complexity of boson sampling. For single-photon [39, 40] and gaussian boson sampling [42], when $N_{\text{out}} \propto \sqrt{N}$ photons survive before measurement, classical state approximation of the output state provides an efficient method of simulation. However, the approximation error of these methods is fixed for given parameters and cannot be controlled with more resources. To overcome this limitation for single-photon boson sampling, tensor network methods that allow us to control the simulation error by tuning time and memory have been used to numerically show the logarithmic scaling of the operator EE in the number of input photons N for the same photon survival scaling [55]. Therefore, what remains unknown is the operator EE scaling of GBS, which is more experimentally relevant, as well as potential boson sampling schemes with alternative photon sources. It was particularly challenging to investigate the EE scaling for GBS because of the infinite-dimensional local Hilbert space for each squeezed mode, which remains high even under suitable truncation and leads to dramatically increased computational cost.

In this work, we develop a hardware-accelerated tensor network algorithm that allows us to simulate previously intractable systems such as GBS with today’s computing resources using tensor networks, giving us the ability to access the quantum state instead of only sampling bit strings. We show the operator EE scaling of GBS under various loss conditions and verify its logarithmic scaling under the same $N_{\text{out}} \propto \sqrt{N}$ condition as single photon boson sampling (SPBS). We also show analytically that in the asymptotic limit of large N , the logarithmic operator EE scaling holds for $N_{\text{out}} \propto \sqrt{N}$ independent of the input photon state. Combined with our numerical result relating MPO EE and the bond dimension, our work suggests that boson sampling with loss higher than the aforementioned scaling may be efficiently simulated with tensor networks as

the system size grows.

II. RESULTS

A. Matrix product operator algorithm with $U(1)$ symmetry on GPU

Lossy quantum states in boson sampling can be represented by matrix product states (MPSs) and matrix product operators (MPOs) [55, 56]. More explicitly, given an M -body pure state

$$|\Psi\rangle = \sum_{i_1, \dots, i_M=0}^{d-1} c_{i_1, \dots, i_M} |i_1, \dots, i_M\rangle, \quad (1)$$

the corresponding MPS is

$$c_{i_1, \dots, i_M} = \sum_{\alpha_0, \dots, \alpha_M=0}^{\chi-1} \Gamma_{\alpha_0 \alpha_1}^{[1]i_1} \lambda_{\alpha_1}^{[1]} \Gamma_{\alpha_1 \alpha_2}^{[2]i_2} \lambda_{\alpha_2}^{[2]} \times \dots \lambda_{\alpha_{M-1}}^{[M-1]} \Gamma_{\alpha_{M-1} \alpha_M}^{[M]i_M}, \quad (2)$$

where d is the local Hilbert space dimension and χ is the bond dimension. The tensor c_{i_1, \dots, i_M} fully characterizes the state $|\Psi\rangle$, but is M dimensional with d indices each, leading to M^d entries in storage. The MPS, however, represents this large tensor as a contraction (sum over the dummy or virtual α indices) of a chain of tensors, making it especially suitable for one-dimensional systems. One can observe that the i indices representing the physical degrees of freedom remain open (unsummed). The memory complexity of the MPS is $O(\chi^2 dM)$, and χ can be adjusted to represent c with the desired accuracy. Further, one can efficiently perform local unitary operations on the MPS and calculate expectation values of local observables with complexity $O(d^4 \chi^3)$, allowing efficient simulation of one-dimensional systems.

The MPS formulation is especially convenient for quantifying entanglement. If we perform the Schmidt decomposition on the quantum state, which is to express the wavefunction as the sum of tensor products of states of two subsystems A and B

$$|\Psi\rangle = \sum_{\alpha} \lambda_{\alpha} |\alpha_A\rangle |\alpha_B\rangle, \quad (3)$$

where $\{|\alpha\rangle\}$ forms a basis set for each subsystem, we reveal the entanglement between the two subsystems, and the entanglement entropy (EE) given by

$$- \sum_{\alpha} \lambda_{\alpha}^2 \log \lambda_{\alpha}^2 \quad (4)$$

quantifies how much entanglement there is. Conveniently, if the subsystems are bipartitions of the MPS at site ℓ , the λ_{α} ’s would be $\lambda_{\alpha_{\ell}}^{[\ell]}$, allowing us to compute the MPS EE. For a mixed state described by the density operator $\hat{\rho}$, we can flatten it into a d^2 dimensional vector, and the corresponding tensor network representation analogous to E.q. 2 is the MPO. We can

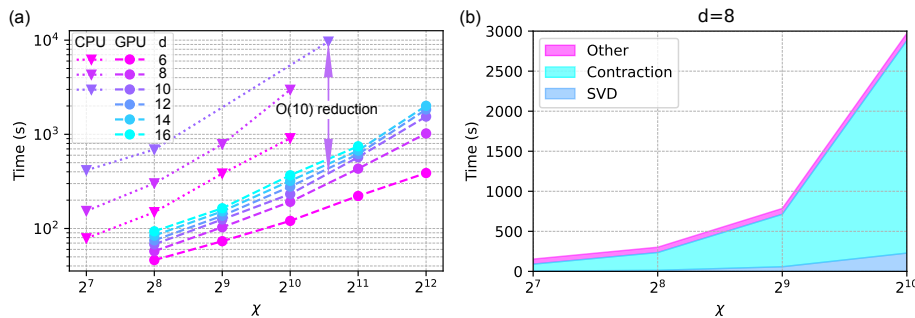


Figure 1. Simulation time of the CPU algorithm and GPU algorithm. (a) CPU algorithm time compared to GPU algorithm time. Dotted triangle marker traces are for the CPU algorithm, and dashed circular marker traces are for the GPU algorithm. We observe a reduction of time on the order of tenfold. (b) Contribution to simulation time of the CPU algorithm from subroutines with local Hilbert space size $d = 8$.

formally perform Schmidt decomposition on the vectorized mixed state, identify the singular values λ_α with $\lambda_{\alpha_\ell}^{[\ell]}$ in the MPO representation, and similarly compute the MPO EE.

For systems with large local dimensions d , the $O(d^4\chi^3)$ computational complexity becomes significant. For mixed state simulations with MPOs, the complexity becomes $O(d^8\chi^3)$, which is especially problematic for systems with large d such as GBS. Fortunately, for systems with global symmetry, such as particle number or total spin conservation, another level of reduction is possible. Symmetry preserving operators can be expressed as a direct sum $\hat{T} = \bigoplus_n \hat{T}_n$ where \hat{T}_n preserves the subspace \mathbb{V}_n corresponding to some conserved charge n , and tensors can be therefore written in a block diagonal form and stored efficiently [57]. Computations are performed on different blocks independently, and the time cost also reduces due to the non-linear polynomial complexity.

To update the MPO according to the action of a beam splitter, two tensors of the nearby sites are updated by contracting with the unitary, followed by a singular value decomposition (SVD). All steps are performed on each of the d^2 charge blocks independently, hence the significantly reduced SVD cost. However, due to the $U(1)$ symmetric form of the MPO, the contraction step is far more complex than regular tensor contraction. This prevents the algorithm from exploiting highly optimized modern computational software and hardware infrastructures developed for common array and tensor manipulations, and the time cost of contraction dominates that of SVD. Specifically, the CPU implementation loops over all left, middle, and right charges, leading to an $O(d^6)$ complexity. We implement an efficient custom graphics processing unit (GPU) kernel that processes all left and right charges in parallel and borrows optimization techniques from matrix multiplication. This effectively reduces the relative time of contraction to zero compared to SVD. The SVD subroutine is further accelerated by the GPU, making the overall run time even shorter.

Lossy boson sampling can be simulated using this algorithm. In the case where loss is uniform, although lossy channels do not preserve photon numbers and are therefore not $U(1)$ symmetric, we can move all losses to the initial state since loss commutes with linear optical transformations. As a result, full Kraus operator-based simulation of noisy channels is not

necessary, and we can update our MPO state by vectorization and applying $U(1)$ symmetric unitaries [56–58]. This reduces the memory footprint of the MPO by a factor of d^2 , and the GPU implementation further eliminates the need to loop over left and right charges. This is more significant for GBS than SPBS due to the infinite number of Fock states per mode and the higher truncation dimension required. Our GPU algorithm is necessary for studying GBS systems of moderate sizes.

We show the reduction in time-to-solution by using our GPU algorithm in Fig. 1 a. We show that the CPU-based algorithm is much slower, and contraction takes up most of the computational time as shown in Fig. 1 b. Details on GPU timing can be found in Supplementary Figures.

B. Asymptotic MPO entanglement entropy scaling for boson sampling

The quantum state of N independent and identical modes can be written as

$$|\psi_{\text{in}}\rangle = \bigotimes_{j=1}^N \left(\sum_{n=0}^{\infty} c_n \frac{\hat{a}_j^{\dagger n}}{\sqrt{n!}} \right) |0\rangle, \quad (5)$$

where \hat{a}_j^{\dagger} is the input creation operator. The action of an M -mode beam splitter array is to transform the input state into

$$|\psi_{\text{out}}\rangle = \bigotimes_{j=1}^N \sum_{n=0}^{\infty} c_n \sum_{k_j=0}^n \sqrt{\frac{n!}{k!(n-k)!}} \cos^{k_j} \theta_j \sin^{n-k_j} \theta_j |k_j\rangle_{\text{up},j} |n-k_j\rangle_{\text{down},j}, \quad (6)$$

where $\theta_j, |k_j\rangle_{\text{side},j}$ are related to the unitary matrix representing the interferometer. This formalism allows us to calculate the MPO EE without explicitly constructing the output state given the unitary representing the interferometer. Specifically, the details of the unitary matrix are hidden in the $|k\rangle_{\text{side},j}$ states constructed to satisfy orthogonality. The coefficients $\cos^2 \theta_j, \sin^2 \theta_j$ related to the unitary can also be simply approximated as $\frac{1}{2}$ in the asymptotic limit of large M if l is chosen to be $\frac{M}{2}$. This choice of bipartition should produce the

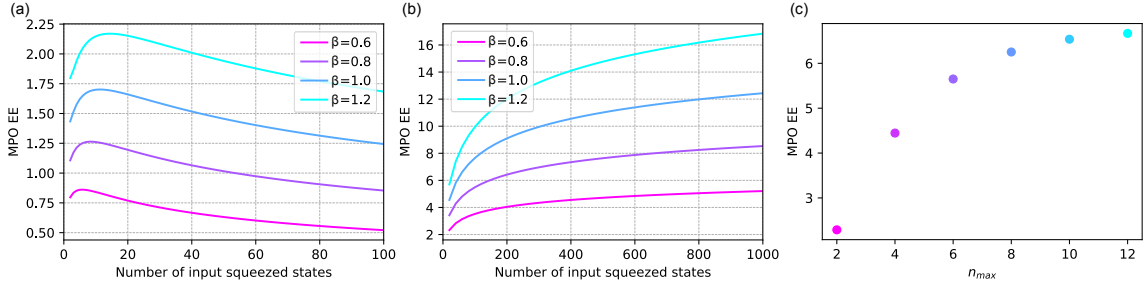


Figure 2. Operator entanglement entropy vs. the number of input squeezed modes for different photon survival scaling $N_{\text{out}} = \beta N^\gamma$ at $r = 0.88$. (a) $\gamma = \frac{1}{4}$. (b) $\gamma = \frac{1}{2}$. (c) Convergence of MPO EE with increasing n_{max} for $N = 50$, $\beta = 1$, $\gamma = \frac{1}{2}$, $r = 0.88$.

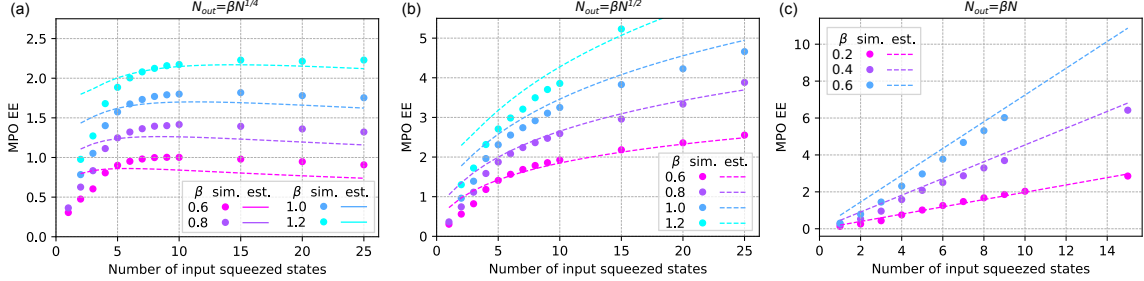


Figure 3. Operator entanglement entropy vs. the number of input squeezed modes for different photon survival scaling $N_{\text{out}} = \beta N^\gamma$ at $r = 0.88$. Details of experiment configurations can be found in Methods. (a) $\gamma = \frac{1}{4}$. (b) $\gamma = \frac{1}{2}$. (c) $\gamma = 1$. Dots are results obtained from full simulations using $U(1)$ symmetry. Dashed lines are estimates using asymptotic assumptions.

largest MPO EE.

Analytically, we derive the MPO EE in the limit of large N . In this case, details of the input photon state are no longer relevant in the scaling analysis, and we derive that

$$S_1 = O(N^{2\gamma-1} \log N), \quad (7)$$

where $\mu \rightarrow \beta N^\gamma / N$ is the photon survival rate. This leads to the $\gamma = \frac{1}{2}$ threshold for logarithmic MPO EE scaling.

C. Numerical experiments

We show the MPO EE scaling in the number of input squeezed modes for different photon survival scaling, estimated using both asymptotic forms and full simulations using $U(1)$ symmetry. Specifically, we examine photon survival scaling $N_{\text{out}} \propto N^\gamma$ with $\gamma = \frac{1}{4}, \frac{1}{2}, 1$. To make a fair comparison against SPBS, the squeezing parameter is fixed at $r = 0.88$, which averages to approximately one photon per squeezed mode. The wavefunction for a single squeezed mode and its corresponding output wavefunction, which are the GBS case of E.q. 5 and E.q. 6, are given by:

$$|\psi_{\text{in}}\rangle = \frac{1}{\sqrt{\cosh r}} \sum_{n=0}^{n_{\text{max}}/2} \frac{\tanh^n r}{2^{2n}} \hat{a}^{\dagger 2n} |0\rangle \quad (8)$$

$$\rightarrow |\psi_{\text{out}}\rangle = \frac{1}{\sqrt{\cosh r}} \sum_{n=0}^{n_{\text{max}}/2} \frac{\tanh^n r (2n)!}{2^{2n}} \sum_k \frac{\cos^k \theta \sin^{2n-k} \theta}{\sqrt{k!(2n-k)!}} |k\rangle_{\text{up}} |2n-k\rangle_{\text{down}}. \quad (9)$$

Fig. 2 shows the asymptotic estimates with $n_{\text{max}} = 8$ for large system sizes. Similar to what is observed in SPBS simulations, GBS shows MPO EE reduction when the loss is sufficiently high for $\gamma = \frac{1}{4}$, logarithmic scaling for $\gamma = \frac{1}{2}$, and linear scaling for $\gamma = 1$ (Fig.3 c). A similar linear increase in MPO EE with β is also observed in all three cases. Further, we also show the numerical convergence of our asymptotic MPO EE estimates by increasing the cut-off of the initial maximum photon number n_{max} for the squeezed states.

Further, the full simulations and asymptotic forms agree quantitatively, as shown in Fig. 3. However, we observe that the quality of agreement is poor when MPO EE is small such as in many $\gamma = \frac{1}{4}$ data points when the number of input squeezed states N is small. In the regime of small MPO EE but large N , we attribute the disagreement to the formal differences between regular MPOs and MPOs in a $U(1)$ symmetric form. This is easy to see as even a product state can have non-zero $U(1)$

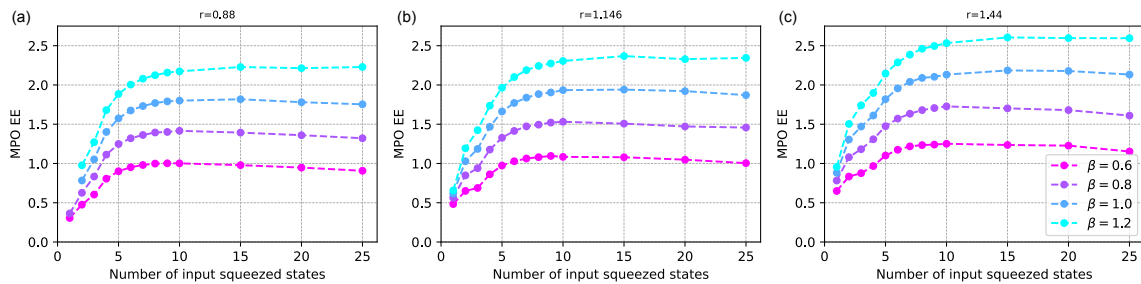


Figure 4. Operator entanglement entropy vs. the number of input squeezed modes for different squeezing parameters r . (a) $r = 0.88$, averaging approximately 1 photon per mode. (b) $r = 1.146$, averaging approximately 2 photons per mode. (c) $r = 1.44$, averaging approximately 4 photons per mode.

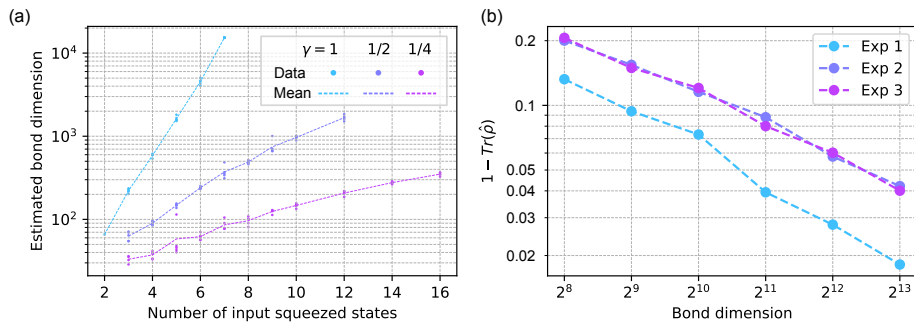


Figure 5. Analysis of bond dimension, system size, and error. Details can be found in Methods. (a) Bond dimension needed to reach accuracy $1 - \text{Tr}(\hat{\rho}) = 0.02$ vs. the number of input squeezed modes photon survival scaling $N_{\text{out}} = 0.4N^\gamma$ at $r = 0.88$. Dots are individual estimates of the bond dimension obtained from full simulations using $U(1)$ symmetry. Dashed lines are the means. (b) Reduction in $1 - \text{Tr}(\hat{\rho})$ error as bond dimension increases for three different experimental configurations.

symmetric MPO EE simply due to the existence of different charges. For small N , we expect the quality of the approximation to be poor because we are no longer in the asymptotic limit. Further disagreement can also be attributed to the fact that the $U(1)$ symmetric full simulations are limited by the bond dimension. We ensure that all plotted data points are simulated to $1 - \text{Tr}(\hat{\rho}) < 0.1$, which previous work established as a good proxy to the total variation error that is computationally lightweight.

Lastly, we investigate the effect of squeezing on MPO EE with our full $U(1)$ symmetric simulations. We choose to investigate $\gamma = \frac{1}{4}$ for easier simulation. Fig. 4 shows an increase in MPO EE with increasing squeezing parameter r . It is important to note that the average number of output photons scales with the average number of input photons N , not the number of squeezed states. This means that for the same number of input squeezed states and β , a higher squeezing parameter has a higher loss. Increasing the average number of photons per squeezed mode from 1 to 2 and 4 only moderately increases the MPO EE compared to increasing N . This observation is similar to the previous finding for Fock state boson sampling: if the number of input modes stays the same and the number of photons per mode increases, the MPO EE grows slowly and can be efficiently simulated [55].

Our numerical findings on the MPO EE growth for different loss scalings have complexity implications, but there is a lack

of rigorous correspondence between MPO EE and simulation time. Although we can formally perform Schmidt decomposition on the vectorized mixed state and identify the singular values with λ 's in the MPO representation, the interpretation of entanglement becomes murkier because of the incorporation of classical correlation in the expression. Further, suitable truncation of the singular values ensures that the 2-norm between the approximate vectorized mixed state and the ideal vectorized mixed state is controlled. However, the bound on the trace distance between the density operators is larger by a factor of the dimension of the Hilbert space. Therefore, when the MPO EE decreases as the system size increases, the required bond dimension to bound the 2-norm decreases, but the required bond dimension to bound the trace distance may still increase.

To make the statement on simulation complexity more rigorous, we validate the entanglement entropy growth explicitly. We show in Fig. 5 the growth of bond dimension in the system size for fixed accuracy of $1 - \text{Tr}(\hat{\rho}) = 0.02$. It is clear that constant loss leads to exponential growth in the bond dimension. In higher loss cases, growth is much more moderate and appears sub-exponential. We also validate that increasing the bond dimension efficiently reduces the simulation error. We choose three experiments and simulated them with different bond dimensions.

III. DISCUSSION

In this work, our use of the state-of-the-art hardware accelerator Nvidia A100 GPU allows symmetric tensor network simulations to exploit the latest advancements in computing technologies and opens up more opportunities to investigate interesting physical systems computationally. Beyond GPUs, other hardware accelerator platforms, such as FPGAs [59] and TPUs [60], could offer additional opportunities. This is made especially approachable with the advent of high-level abstractions for heterogeneous device programming such as SYCL [61]. More important, however, are the scientific opportunities beyond engineering.

It is clear that to experimentally demonstrate hard-to-simulate boson sampling, we must operate in an intermediate regime where the number of photons and entanglement is high enough while the depth of the interferometer is low enough to avoid unfavorable loss. However, the usefulness of the experiments and algorithms that this restriction allows remains an open question. While our tensor network simulation technique allows us to draw a theoretical conclusion regarding the scaling of complexity with respect to loss, new efforts on boson sampling will inevitably try to avoid any type of unfavorable loss scaling and limit the interferometer depth. It is precisely the competition between entanglement generation and photons loss management that future experimental designs will need to optimize, and it will be necessary to classically simulate this interplay to further our understanding in a new era of potentially useful boson sampling.

Although the MPO formalism intrinsically assumes a 1D architecture of the interferometer, the fact that we are simulating Haar random unitaries means that our findings are architecture independent. However, if we want to simulate high dimensional low depth systems that are not Haar random [27, 28], one potential direction to move forward is to adopt more exotic tensor networks such as projected entanglement pair states (PEPS), which is a generalization of our tensor network to higher dimensions. $U(1)$ symmetric forms of generic tensor networks can be constructed in principle [57], and lossy simulations could be achieved by incorporating loss at initialization.

Our approach can be extended to a broader class of physical systems and simulate more exotic quantum phenomena. As is, our approach can be used to extend the capabilities of time evolution and ground state approximation of particle number or spin-preserving one-dimensional chain Hamiltonians and dissipative systems [58], as well as one-dimensional multiparticle quantum walks [62, 63]. For example, multiparticle quantum walks may provide a sensing advantage, and simulations of higher particle number systems with our accelerated algorithm can provide crucial insight. Extending to PEPS can also enable quantum walk simulations in two dimensions, where topological features are far more interesting [64] and novel transport phenomena arise [65]. Overall, our work unleashes the potential of many new exciting frontiers of investigation.

IV. METHODS

We carry out our GPU numerical simulations using the Polaris system at the Argonne Leadership Computing Facility (ALCF). Each node has a single 2.8 GHz AMD EPYC Milan 7543P 32-core CPU with 512 GB of DDR4 RAM and four Nvidia A100 GPUs connected via NVLink. We perform our CPU numerical simulations using the Bebop system at ALCF. Each node has a single 2.10 GHz Intel Xeon E5-2695v4 32-core CPU with 128GB of DDR4 RAM.

All full $U(1)$ symmetric MPO simulations have $M = \max(20, 4N)$ modes, and the local Hilbert space dimension d is chosen such that $< 1\%$ of the probability is truncated. Because the left-most charge is the sum of all photons, the required d is higher for higher squeezing parameters r and higher numbers of input squeezed states. Global Haar random interferometers are used and constructed using an M -layer array [66].

For Fig. 3 and 4, we simulate the system until there is no MPO EE increase for at least 10 layers. This is reasonable since we only care about the maximum MPO EE throughout simulation which captures the computational cost, and the MPO EE generically increases as more depths are simulated until saturation, after which the MPO EE decreases slowly. All data points of MPO EE are obtained by only a single experiment, as we observe that no significant noise is present in our results because we only extract the maximum. We ensure that all plotted data points are simulated to $1 - \text{Tr}(\hat{\rho}) < 0.1$, which previous work established as a good proxy to the total variation error that is computationally lightweight. The largest simulation is for linear scaling simulations with $d = 18, \beta = 0.4, N = 15, M = 60, \chi = 16384$ ran on 10 Polaris nodes with 40 GPUs in total.

For Fig. 5, the full depth of the interferometer is simulated. This is because simulating each layer produces additional error, and therefore affects the required bond dimension. For each configuration in Fig. 5 a, the bond dimension starts with a small value and doubles if the error exceeds 0.02. Once the bond dimension is large enough to exceed the desired accuracy, the bond dimension is refined a few more times to obtain a more precise estimate. For linear scaling and 7 input squeezed states, the simulation is expensive and we verified that setting $\chi = 15296$ produced $1 - \text{Tr}(\hat{\rho}) = 0.020, 0.022, 0.021, 0.021, 0.019$ across 5 different experiments and used 15296 as the estimated bond dimension. The three experiments for Fig. 5 b are $M = 10, 15, 20$ and $\mu = 0.2, 0.15, 0.1$ respectively, and each data point is obtained from one simulation.

DATA AVAILABILITY

Data used to generate the figures are available upon request from the authors.

CODE AVAILABILITY

The code used to generate the data and figures is available in the GitHub repository <https://github.com/sss441803/BosonSampling>.

ACKNOWLEDGEMENTS

This research has been supported by and has used the resources of the Argonne Leadership Computing Facility, which is a U.S. Department of Energy (DOE) Office of Science User Facility supported under Contract DE-AC02-06CH11357. Y. A. acknowledges support from the U.S. Department of Energy, Office of Science, under contract DE-AC02-06CH11357 at Argonne National Laboratory and Defense Advanced Research Projects Agency (DARPA) under Contract No. HR001120C0068. L. J. acknowledges support from the the ARO (W911NF-23-1-0077), ARO MURI (W911NF-21-1-0325), AFOSR MURI (FA9550-19-1-0399, FA9550-21-1-0209), AFRL (FA8649-21-P-0781), DoE Q-NEXT, NSF (OMA-1936118, ERC-1941583, OMA-2137642), NTT Research, and the Packard Foundation (2020-71479). J. L. is supported in part by International Business Machines (IBM) Quantum through the Chicago Quantum Exchange, and the Pritzker School of Molecular Engineering at the University of Chicago through AFOSR MURI (FA9550-21-1-0209).

M. L. acknowledges support from DOE Q-NEXT. C. O. acknowledges support from the the ARO (W911NF-23-1-0077), ARO MURI (W911NF-21-1-0325), AFOSR MURI (FA9550-19-1-0399, FA9550-21-1-0209), AFRL (FA8649-21-P-0781), DoE Q-NEXT, NSF (OMA-1936118, ERC-1941583, OMA-2137642), NTT Research, and the Packard Foundation (2020-71479).

V. COMPETING INTERESTS

The authors declare no competing financial or non-financial interests.

VI. AUTHOR CONTRIBUTIONS

M.L. developed the majority of the software, performed all numerical simulations and theoretical derivations, and wrote the majority of the manuscript. C.O. provided the original CPU implementation, developed the MPO initialization scheme, performed preliminary theoretical work, and contributed significantly to manuscript editing. All other authors contributed novel ideas, provided numerous scientific and writing improvements about the paper, and participated in discussions that shaped the project in a substantial manner and the understanding of its broader impact.

-
- [1] P. W. Shor, “Algorithms for quantum computation: discrete logarithms and factoring,” in *Proceedings 35th annual symposium on foundations of computer science* (Ieee, 1994) pp. 124–134.
- [2] Lov K. Grover, “A fast quantum mechanical algorithm for database search,” in *Proceedings of the Twenty-Eighth Annual ACM Symposium on Theory of Computing*, STOC ’96 (Association for Computing Machinery, New York, NY, USA, 1996) p. 212–219.
- [3] Aram W. Harrow, Avinatan Hassidim, and Seth Lloyd, “Quantum algorithm for linear systems of equations,” *Phys. Rev. Lett.* **103**, 150502 (2009).
- [4] D. W. Berry, G. Ahokas, R. Cleve, and B. C. Sanders, “Efficient quantum algorithms for simulating sparse hamiltonians,” *Commun. Math. Phys.* **270**, 359–371 (2007).
- [5] Dominic W. Berry, Andrew M. Childs, Richard Cleve, Robin Kothari, and Rolando D. Somma, “Exponential improvement in precision for simulating sparse hamiltonians,” in *Proceedings of the Forty-Sixth Annual ACM Symposium on Theory of Computing*, STOC ’14 (Association for Computing Machinery, New York, NY, USA, 2014) p. 283–292.
- [6] A.M. Childs, “On the relationship between continuous- and discrete-time quantum walk,” *Commun. Math. Phys.* **294**, 581–603 (2010).
- [7] Guang Hao Low and Isaac L. Chuang, “Optimal hamiltonian simulation by quantum signal processing,” *Phys. Rev. Lett.* **118**, 010501 (2017).
- [8] Yuri Alexeev, Dave Bacon, Kenneth R. Brown, Robert Calderbank, Lincoln D. Carr, Frederic T. Chong, Brian DeMarco, Dirk Englund, Edward Farhi, Bill Fefferman, Alexey V. Gorshkov, Andrew Houck, Jungsang Kim, Shelby Kimmel, Michael Lange, Seth Lloyd, Mikhail D. Lukin, Dmitri Maslov, Peter Maunz, Christopher Monroe, John Preskill, Martin Roetteler, Martin J. Savage, and Jeff Thompson, “Quantum computer systems for scientific discovery,” *PRX Quantum* **2** (2021), 10.1103/prxquantum.2.017001.
- [9] M. A. Broome, A. Fedrizzi, S. Rahimi-Keshari, J. Dove, S. Aaronson, T. C. Ralph, and A. G. White, “Photonic boson sampling in a tunable circuit,” *Science* **339**, 794–798 (2013).
- [10] J. B. Spring, B. J. Metcalf, P. C. Humphreys, W. S. Kolthammer, X.-M. Jin, M. Barbieri, A. Datta, N. Thomas-Peter, N. K. Langford, D. Kundys, *et al.*, “Boson sampling on a photonic chip,” *Science* **339**, 798–801 (2013).
- [11] M. Tillmann, B. Dakić, R. Heilmann, S. Nolte, A. Szameit, and P. Walther, “Experimental boson sampling,” *Nat. Photonics* **7**, 540–544 (2013).
- [12] A. Crespi, R. Osellame, R. Ramponi, D. J. Brod, E. F. Galvao, N. Spagnolo, C. Vitelli, E. Maiorino, P. Mataloni, and F. Sciarrino, “Integrated multimode interferometers with arbitrary designs for photonic boson sampling,” *Nat. Photonics* **7**, 545–549 (2013).
- [13] N. Spagnolo, C. Vitelli, M. Bentivegna, D. J. Brod, A. Crespi, F. Flamini, S. Giacomini, G. Milani, R. Ramponi, P. Mataloni, *et al.*, “Experimental validation of photonic boson sampling,” *Nat. Photonics* **8**, 615–620 (2014).
- [14] J. Carolan, J. D. A. Meinecke, P. J. Shadbolt, N. J. Russell, N. Ismail, K. Wörhoff, T. Rudolph, M. G. Thompson, J. L. O’Brien, J. C. F. Matthews, *et al.*, “On the experimental verification of quantum complexity in linear optics,” *Nat. Photonics* **8**, 621–626 (2014).

- [15] J. Carolan, C. Harrold, C. Sparrow, E. Martín-López, N. J. Russell, J. W. Silverstone, P. J. Shadbolt, N. Matsuda, M. Oguma, M. Itoh, *et al.*, “Universal linear optics,” *Science* **349**, 711–716 (2015).
- [16] M. Bentivegna, N. Spagnolo, C. Vitelli, F. Flamini, N. Vigianniello, L. Latmiral, P. Mataloni, D. J. Brod, E. F. Galvão, A. Crespi, *et al.*, “Experimental scattershot boson sampling,” *Sci. Adv.* **1**, e1400255 (2015).
- [17] H.-S. Zhong, Y. Li, W. Li, L.-C. Peng, Z.-E. Su, Y. Hu, Y.-M. He, X. Ding, W. Zhang, H. Li, *et al.*, “12-photon entanglement and scalable scattershot boson sampling with optimal entangled-photon pairs from parametric down-conversion,” *Phys. Rev. Lett.* **121**, 250505 (2018).
- [18] H.-S. Zhong, L.-C. Peng, Y. Li, Y. Hu, W. Li, J. Qin, D. Wu, W. Zhang, H. Li, L. Zhang, Z. Wang, L. You, X. Jiang, L. Li, N.-L. Liu, J. P. Dowling, C.-Y. Lu, and J.-W. Pan, “Experimental Gaussian boson sampling,” *Science Bulletin* **64**, 511–515 (2019).
- [19] S. Paesani, Y. Ding, R. Santagati, L. Chakhmakhchyan, C. Vigiari, K. Rottwitz, L. K. Oxenløwe, J. Wang, M. G. Thompson, and A. Laing, “Generation and sampling of quantum states of light in a silicon chip,” *Nat. Phys.* **15**, 925–929 (2019).
- [20] Y. He, X. Ding, Z.-E. Su, H.-L. Huang, J. Qin, C. Wang, S. Unsleber, C. Chen, H. Wang, Y.-M. He, *et al.*, “Time-bin-encoded boson sampling with a single-photon device,” *Phys. Rev. Lett.* **118**, 190501 (2017).
- [21] J. C. Laredo, M. A. Broome, P. Hilaire, O. Gazzano, I. Sagnes, A. Lemaitre, M. P. Almeida, P. Senellart, and A. G. White, “Boson sampling with single-photon fock states from a bright solid-state source,” *Phys. Rev. Lett.* **118**, 130503 (2017).
- [22] H. Wang, Y. He, Y.-H. Li, Z.-E. Su, B. Li, H.-L. Huang, X. Ding, M.-C. Chen, C. Liu, J. Qin, *et al.*, “High-efficiency multiphoton boson sampling,” *Nat. Photonics* **11**, 361–365 (2017).
- [23] H. Wang, W. Li, X. Jiang, Y.-M. He, Y.-H. Li, X. Ding, M.-C. Chen, J. Qin, C.-Z. Peng, C. Schneider, *et al.*, “Toward scalable boson sampling with photon loss,” *Phys. Rev. Lett.* **120**, 230502 (2018).
- [24] H. Wang, J. Qin, X. Ding, M.-C. Chen, S. Chen, X. You, Y.-M. He, X. Jiang, L. You, Z. Wang, *et al.*, “Boson sampling with 20 input photons and a 60-mode interferometer in a 10^{14} -dimensional hilbert space,” *Phys. Rev. Lett.* **123**, 250503 (2019).
- [25] Han-Sen Zhong, Hui Wang, Yu-Hao Deng, Ming-Cheng Chen, Li-Chao Peng, Yi-Han Luo, Jian Qin, Dian Wu, Xing Ding, Yi Hu, Peng Hu, Xiao-Yan Yang, Wei-Jun Zhang, Hao Li, Yuxuan Li, Xiao Jiang, Lin Gan, Guangwen Yang, Lixing You, Zhen Wang, Li Li, Nai-Le Liu, Chao-Yang Lu, and Jian-Wei Pan, “Quantum computational advantage using photons,” *Science* (2020), 10.1126/science.abe8770.
- [26] Han-Sen Zhong, Yu-Hao Deng, Jian Qin, Hui Wang, Ming-Cheng Chen, Li-Chao Peng, Yi-Han Luo, Dian Wu, Si-Qiu Gong, Hao Su, Yi Hu, Peng Hu, Xiao-Yan Yang, Wei-Jun Zhang, Hao Li, Yuxuan Li, Xiao Jiang, Lin Gan, Guangwen Yang, Lixing You, Zhen Wang, Li Li, Nai-Le Liu, Jelmer J. Renema, Chao-Yang Lu, and Jian-Wei Pan, “Phase-programmable gaussian boson sampling using stimulated squeezed light,” *Phys. Rev. Lett.* **127**, 180502 (2021).
- [27] L. S. Madsen, F. Laudenbach, M. F. Askarani, F. Rortais, T. Vincent, J. F. F. Bulmer, F. M. Miatto, L. Neuhaus, L. G. Helt, M. J. Collins, A. E. Lita, T. Gerrits, S. W. Nam, V. D. Vaidya, M. Menotti, I. Dhand, Z. Vernon, N. Quesada, and J. Lavoie, “Quantum computational advantage with a programmable photonic processor,” *Nature* **606**, 75–81 (2022).
- [28] Abhinav Deshpande, Arthur Mehta, Trevor Vincent, Nicolás Quesada, Marcel Hinsche, Marios Ioannou, Lars Madsen, Jonathan Lavoie, Haoyu Qi, Jens Eisert, Dominik Hangleiter, Bill Fefferman, and Ish Dhand, “Quantum computational advantage via high-dimensional gaussian boson sampling,” *Science Advances* **8**, eabi7894 (2022).
- [29] A. P. Lund, A. Laing, S. Rahimi-Keshari, T. Rudolph, J. L. O’Brien, and T. C. Ralph, “Boson sampling from a gaussian state,” *Phys. Rev. Lett.* **113**, 100502 (2014).
- [30] Sonja Barkhofen, Tim J. Bartley, Linda Sansoni, Regina Kruse, Craig S. Hamilton, Igor Jex, and Christine Silberhorn, “Driven boson sampling,” *Phys. Rev. Lett.* **118**, 020502 (2017).
- [31] L. Chakhmakhchyan and N. J. Cerf, “Boson sampling with gaussian measurements,” *Phys. Rev. A* **96**, 032326 (2017).
- [32] J. Huh, G. G. Guerreschi, B. Peropadre, J. R. McClean, and A. Aspuru-Guzik, “Boson sampling for molecular vibronic spectra,” *Nat. Photonics* **9**, 615–620 (2015).
- [33] C. S. Wang, J. C. Curtis, B. J. Lester, Y. Zhang, Y. Y. Gao, J. Freeze, V. S. Batista, P. H. Vaccaro, I. L. Chuang, L. Frunzio, *et al.*, “Efficient multiphoton sampling of molecular vibronic spectra on a superconducting bosonic processor,” *Phys. Rev. X* **10**, 021060 (2020).
- [34] Kamil Brádler, Pierre-Luc Dallaire-Demers, Patrick Reberntrost, Daiqin Su, and Christian Weedbrook, “Gaussian boson sampling for perfect matchings of arbitrary graphs,” *Phys. Rev. A* **98**, 032310 (2018).
- [35] Leonardo Banchi, Mark Fingerhuth, Tomas Babej, Christopher Ing, and Juan Miguel Arrazola, “Molecular docking with gaussian boson sampling,” *Science Advances* **6**, eaax1950 (2020).
- [36] S. Aaronson and A. Arkhipov, “The computational complexity of linear optics,” in *Proceedings of the forty-third annual ACM symposium on Theory of computing* (2011) pp. 333–342.
- [37] C. S. Hamilton, R. Kruse, L. Sansoni, S. Barkhofen, C. Silberhorn, and I. Jex, “Gaussian boson sampling,” *Phys. Rev. Lett.* **119**, 170501 (2017).
- [38] Regina Kruse, Craig S. Hamilton, Linda Sansoni, Sonja Barkhofen, Christine Silberhorn, and Igor Jex, “Detailed study of gaussian boson sampling,” *Phys. Rev. A* **100**, 032326 (2019).
- [39] M. Oszmaniec and D. J. Brod, “Classical simulation of photonic linear optics with lost particles,” *New J. Phys.* **20**, 092002 (2018).
- [40] R. García-Patrón, J. J. Renema, and V. Shchesnovich, “Simulating boson sampling in lossy architectures,” *Quantum* **3**, 169 (2019).
- [41] J. Renema, V. Shchesnovich, and R. Garcia-Patron, “Classical simulability of noisy boson sampling,” arXiv preprint arXiv:1809.01953 (2018).
- [42] Haoyu Qi, Daniel J. Brod, Nicolás Quesada, and Raúl García-Patrón, “Regimes of classical simulability for noisy Gaussian boson sampling,” *Phys. Rev. Lett.* **124**, 100502 (2020).
- [43] Abhinav Deshpande, Bill Fefferman, Minh C. Tran, Michael Foss-Feig, and Alexey V. Gorshkov, “Dynamical phase transitions in sampling complexity,” *Phys. Rev. Lett.* **121**, 030501 (2018).
- [44] Changhun Oh, Youngrong Lim, Bill Fefferman, and Liang Jiang, “Classical simulation of boson sampling based on graph structure,” *Phys. Rev. Lett.* **128**, 190501 (2022).
- [45] Dorit Aharonov, Michael Ben-Or, Russell Impagliazzo, and Noam Nisan, “Limitations of noisy reversible computation,” arXiv preprint quant-ph/9611028 (1996).
- [46] Frank Arute, Kunal Arya, Ryan Babbush, Dave Bacon, Joseph C Bardin, Rami Barends, Rupak Biswas, Sergio Boixo, Fernando GSL Brandao, David A Buell, *et al.*, “Quantum supremacy using a programmable superconducting processor,” *Nature* **574**, 505–510 (2019).
- [47] K. Noh, L. Jiang, and B. Fefferman, “Efficient classical simulation of noisy random quantum circuits in one dimension,” *Quantum* **4**, 318 (2020).

- [48] Meng Zhang, Chao Wang, Shaojun Dong, Hao Zhang, Yongjian Han, and Lixin He, “Entanglement entropy scaling of noisy random quantum circuits in two dimensions,” arXiv preprint arXiv:2205.13999 (2022).
- [49] Dorit Aharonov, Xun Gao, Zeph Landau, Yunchao Liu, and Umesh Vazirani, “A polynomial-time classical algorithm for noisy random circuit sampling,” arXiv preprint arXiv:2211.03999 (2022).
- [50] Changhun Oh, Liang Jiang, and Bill Fefferman, “On classical simulation algorithms for noisy boson sampling,” arXiv preprint arXiv:2301.11532 (2023).
- [51] Malte C Tichy, “Sampling of partially distinguishable bosons and the relation to the multidimensional permanent,” *Physical Review A* **91**, 022316 (2015).
- [52] Jelmer J Renema, Adrian Menssen, William R Clements, Gil Triginer, William S Kolthammer, and Ian A Walmsley, “Efficient classical algorithm for boson sampling with partially distinguishable photons,” *Physical review letters* **120**, 220502 (2018).
- [53] Valery S Shchesnovich, “Noise in boson sampling and the threshold of efficient classical simulatability,” *Physical Review A* **100**, 012340 (2019).
- [54] Alexandra E Moylett, Raúl García-Patrón, Jelmer J Renema, and Peter S Turner, “Classically simulating near-term partially-distinguishable and lossy boson sampling,” *Quantum Science and Technology* **5**, 015001 (2019).
- [55] Changhun Oh, Kyungjoo Noh, Bill Fefferman, and Liang Jiang, “Classical simulation of lossy boson sampling using matrix product operators,” *Phys. Rev. A* **104**, 022407 (2021).
- [56] H.-L. Huang, W.-S. Bao, and C. Guo, “Simulating the dynamics of single photons in boson sampling devices with matrix product states,” *Phys. Rev. A* **100**, 032305 (2019).
- [57] S. Singh, R. N. C. Pfeifer, and G. Vidal, “Tensor network states and algorithms in the presence of a global $U(1)$ symmetry,” *Phys. Rev. B* **83**, 115125 (2011).
- [58] C. Guo and D. Poletti, “Matrix product states with adaptive global symmetries,” *Phys. Rev. B* **100**, 134304 (2019).
- [59] Ahmad Shawahna, Sadiq M. Sait, and Aiman El-Maleh, “Fpga-based accelerators of deep learning networks for learning and classification: A review,” *IEEE Access* **7**, 7823–7859 (2019).
- [60] Norman P. Jouppi *et al.*, “In-datacenter performance analysis of a tensor processing unit,” in *Proceedings of the 44th Annual International Symposium on Computer Architecture, ISCA '17* (Association for Computing Machinery, New York, NY, USA, 2017) p. 1–12.
- [61] Ruymán Reyes, Gordon Brown, Rod Burns, and Michael Wong, “Sycl 2020: More than meets the eye,” in *Proceedings of the International Workshop on OpenCL, IWOCCL '20* (Association for Computing Machinery, New York, NY, USA, 2020).
- [62] Andrew M. Childs, David Gosset, and Zak Webb, “Universal computation by multiparticle quantum walk,” *Science* **339**, 791–794 (2013).
- [63] Xiaoming Cai, Hongting Yang, Hai-Long Shi, Chaohong Lee, Natan Andrei, and Xi-Wen Guan, “Multiparticle quantum walks and fisher information in one-dimensional lattices,” *Phys. Rev. Lett.* **127**, 100406 (2021).
- [64] Andreas Schreiber, Aurél Gábris, Peter P. Rohde, Kaisa Laiho, Martin Štefaňák, Václav Potoček, Craig Hamilton, Igor Jex, and Christine Silberhorn, “A 2d quantum walk simulation of two-particle dynamics,” *Science* **336**, 55–58 (2012).
- [65] Janos K. Asboth and Jonathan M. Edge, “Edge-state-enhanced transport in a two-dimensional quantum walk,” *Phys. Rev. A* **91**, 022324 (2015).
- [66] Nicholas J Russell, Levon Chakhmakhchyan, Jeremy L O’Brien, and Anthony Laing, “Direct dialling of haar random unitary matrices,” *New Journal of Physics* **19**, 033007 (2017).

Supplementary Materials of Complexity of Gaussian boson sampling with tensor networks

Minzhao Liu,^{1,2} Changhun Oh,³ Junyu Liu,^{3,4,5,6,7,8} Liang Jiang,^{3,5} and Yuri Alexeev^{2,4,5}

¹*Department of Physics, The University of Chicago, Chicago, IL 60637, USA*

²*Computational Science Division, Argonne National Laboratory, Lemont, IL 60439, USA*

³*Pritzker School of Molecular Engineering, The University of Chicago, Chicago, IL 60637, USA*

⁴*Department of Computer Science, The University of Chicago, Chicago, IL 60637, USA*

⁵*Chicago Quantum Exchange, Chicago, IL 60637, USA*

⁶*Kadanoff Center for Theoretical Physics, The University of Chicago, Chicago, IL 60637, USA*

⁷*qBraid Co., Chicago, IL 60615, USA*

⁸*SeQure, Chicago, IL 60615, USA*

I. SUPPLEMENTARY METHODS

A. MPS boson sampling simulations using $U(1)$ symmetry

For simplicity, we discuss the simulation schemes with matrix product states (MPS). Generalization to MPO is discussed later. Consider an M -mode beam splitter array with N input photons. The wavefunction is

$$|\psi\rangle = \sum_{i_1, \dots, i_M=0}^{d-1} c_{i_1, \dots, i_M} |i_1, \dots, i_M\rangle, \quad (\text{I.1})$$

where state $|i_1, \dots, i_M\rangle$ has i_1 photons in mode 1, \dots , and i_M photons in mode M . Using the canonicalized MPS formalism, the c_{i_1, \dots, i_M} probability amplitude tensor can be represented efficiently as

$$c_{i_1, \dots, i_M} = \sum_{\alpha_0, \dots, \alpha_M=0}^{\chi-1} \Gamma_{\alpha_0 \alpha_1}^{[1]i_1} \lambda_{\alpha_1}^{[1]} \Gamma_{\alpha_1 \alpha_2}^{[2]i_2} \lambda_{\alpha_2}^{[2]} \dots \lambda_{\alpha_{M-1}}^{[M-1]} \Gamma_{\alpha_{M-1} \alpha_M}^{[M]i_M}, \quad (\text{I.2})$$

where α_k is the bond index for mode k , and χ is the bond dimension.

Since photon number is conserved, unitary evolutions must obey $U(1)$ symmetry. One can reduce the resources needed further by explicitly constraining the allowed photon numbers. We denote the total number of photons to the right of mode k corresponding to bond α_k as $c_{\alpha_k}^{[k]}$, and

$$c_{i_1, \dots, i_M} = \sum_{\alpha_0, \dots, \alpha_M=0}^{\chi-1} \Gamma_{\alpha_0 \alpha_1}^{[1]} \lambda_{\alpha_1}^{[1]} \Gamma_{\alpha_1 \alpha_2}^{[2]} \dots \lambda_{\alpha_{M-1}}^{[M-1]} \Gamma_{\alpha_{M-1} \alpha_M}^{[M]} \prod_{k=1}^M \delta \left(c_{\alpha_{k-1}}^{[k-1]} - c_{\alpha_k}^{[k]} - i_k \right). \quad (\text{I.3})$$

If a unitary evolution is applied between mode k and $k+1$, the corresponding unitary is

$$\langle i_k, i_{k+1} | U | j_k, j_{k+1} \rangle = U_{j_k, j_{k+1}}^{i_k, i_{k+1}}. \quad (\text{I.4})$$

Updating the wavefunction according to the unitary can be done by the following procedure. First, obtain the Θ tensor through

$$\begin{aligned} \Theta_{\alpha_{k-1} \alpha_{k+1}}^{i_k, i_{k+1}}(c^k) &= \sum_{j_k, j_{k+1}=0}^{d-1} \sum_{\alpha_k=0}^{\chi-1} U_{j_k, j_{k+1}}^{i_k, i_{k+1}} \lambda_{\alpha_{k-1}}^{[k-1]} \Gamma_{\alpha_{k-1} \alpha_k}^{[k]} \lambda_{\alpha_k}^{[k]} \Gamma_{\alpha_k \alpha_{k+1}}^{[k+1]} \lambda_{\alpha_{k+1}}^{[k+1]} \\ &\quad \times \delta \left(c_{\alpha_{k-1}}^{[k-1]} - c_{\alpha_k}^{[k]} - j_k \right) \delta \left(c_{\alpha_k}^{[k]} - c_{\alpha_{k+1}}^{[k+1]} - j_{k+1} \right) \\ &\quad \times \delta \left(c_{\alpha_{k-1}}^{[k-1]} - c_{\alpha_k}^{[k]} - i_k \right) \delta \left(c_{\alpha_k}^{[k]} - c_{\alpha_{k+1}}^{[k+1]} - i_{k+1} \right), \end{aligned} \quad (\text{I.5})$$

where $0 \leq c_{\alpha_k}^{[k]} \leq N$. Singular value decompositions are then performed on $\Theta(c^{[k]})$, and the largest χ singular values out of the singular values for all $\Theta(c^{[k]})$ and their corresponding bonds are retained. The produced outputs are manipulated to update the MPS representation.

B. Adaptation to MPO Gaussian boson sampling

To simulate lossy boson sampling, we use matrix product operators. The formal description of the MPO algorithm can be found in [1]. In summary, MPOs are vectorized into the MPS form, $U \rightarrow U \otimes U^*$, and two conserved charges are present. The CPU implementation of the algorithm now requires loops over two sets of conserved charges, which greatly increases the complexity for large d . The required d is also larger in the gaussian case since squeezed states are superpositions of an infinite number of Fock states. Therefore, the advantage of our GPU implementation is more pronounced in this setting.

C. Asymptotic behaviors of MPO entanglement entropy

The quantum state of N independent and identical modes can be written as:

$$|\psi_{\text{in}}\rangle = \otimes_{j=1}^N \left(\sum_{n=0}^{\infty} c_n \frac{\hat{a}_j^{\dagger n}}{\sqrt{n!}} \right) |0\rangle, \quad (\text{I.6})$$

where \hat{a}_j^{\dagger} is the input creation operator. The action of an M -mode beam splitter array is to transform input creation operators:

$$\hat{a}_j^{\dagger} \rightarrow \cos \theta_j \hat{B}_{\text{up},j}^{\dagger} + \sin \theta_j \hat{B}_{\text{down},j}^{\dagger}, \quad (\text{I.7})$$

where

$$\hat{B}_{\text{side},j}^{\dagger k} |0\rangle = \frac{|k\rangle_{\text{side},j}}{\sqrt{k!}}, \text{ side} \in \{\text{up}, \text{down}\}, \quad (\text{I.8})$$

$$\cos^2 \theta_j = \sum_{k=1}^l |U_{jk}|^2, \sin^2 \theta_j = \sum_{k=l+1}^M |U_{jk}|^2, \quad (\text{I.9})$$

l is the bipartition mode we will use to calculate the MPO entanglement entropy, and $\hat{B}_{\text{side},j}^{\dagger}$ are output creation operators for each bipartition. The output state is

$$|\psi_{\text{out}}\rangle = \otimes_{j=1}^N \sum_{n=0}^{\infty} c_n \sum_{k_j=0}^n \sqrt{\frac{n!}{k!(n-k)!}} \cos^{k_j} \theta_j \sin^{n-k_j} \theta_j |k_j\rangle_{\text{up},j} |n-k_j\rangle_{\text{down},j}. \quad (\text{I.10})$$

The entanglement entropy of this product state is additive over input modes j , and from now on we only focus on a single j and omit this symbol.

The single input mode density operator thus far without loss is

$$\hat{\rho} = \sum_{n=0}^{\infty} \sum_{k_j=0}^n c_{n,k} |k, n-k\rangle \langle k, n-k|, \quad (\text{I.11})$$

and it will have a certain amount of entanglement entropy. The full system, therefore, has entropy linear in N due to the additive nature, and classical simulation of lossless boson sampling is always inefficient in N .

However, with loss, the entanglement entropy can scale differently. Consider the single-body loss channel defined by the Kraus operators

$$\hat{\rho} \rightarrow \sum_{n_{\text{loss}}=0}^{n_{\text{max}}} K^{(n_{\text{loss}})} \hat{\rho} K^{(n_{\text{loss}})\dagger}, \quad (\text{I.12})$$

$$K_{n_{\text{out}}+1, n_{\text{in}}+1}^{(n_{\text{loss}})} = \begin{cases} i \binom{n_{\text{in}}}{n_{\text{out}}} \mu^{n_{\text{out}}} (1-\mu)^{n_{\text{loss}}} & \text{if } n_{\text{in}} - n_{\text{out}} = n_{\text{loss}} \\ 0 & \text{otherwise,} \end{cases} \quad (\text{I.13})$$

where $K^{(n_{\text{loss}})} \in \mathbb{C}^{n_{\text{max}}+1, n_{\text{max}}+1}$ captures processes that lose n_{loss} photons, and we have chosen to limit the maximum photon number to n_{max} .

Our density operator has two partitions, and therefore its loss channel is captured by tensor products of the single-mode Kraus operators. Since the first column corresponding to $n_{\text{out}} = 0$ is strictly composed of powers of $1 - \mu$ for all single mode

Kraus operators, the same must be true for their tensor products. Therefore, all entries of the first column must be of the form $a + b\mu + O(\mu^2)$. As a result, the element on the first row and column of the resulting density operator after the action of the quantum channel must be of the form $a + b\mu + O(\mu^2)$.

Similarly, all other columns of all single-mode Kraus operators must not have constant terms since $n_{\text{out}} > 0$, the same must be true for their tensor products. Therefore, in the limit of small μ , the result density operator is of order

$$\hat{\rho} = \begin{bmatrix} O(1) & O(\mu) & O(\mu) & \cdots \\ O(\mu) & O(\mu^2) & O(\mu^2) & \vdots \\ O(\mu) & O(\mu^2) & O(\mu^2) & \vdots \\ \vdots & \cdots & \cdots & \ddots \end{bmatrix}. \quad (\text{I.14})$$

To compute the MPO entanglement entropy, we need to vectorize the density operator to obtain $|\hat{\rho}\rangle\rangle$, take the outer product to find the corresponding density operator $|\hat{\rho}\rangle\rangle\langle\langle\hat{\rho}|$, take the partial trace over the down bipartition to obtain $\hat{\rho}' = |\hat{\rho}\rangle\rangle\langle\langle\hat{\rho}|_{\text{up}}$, find its eigenvalues, normalize the eigenvalues (vectorized density operator is no longer of unit trace), and compute the entropy. It can be shown that the reduced density operator $\hat{\rho}'$ has the same order as $\hat{\rho}$. Therefore, to the first order, $\hat{\rho}'$ has the form

$$\hat{\rho}' = \begin{bmatrix} \hat{\rho}'_{1,1} & \hat{\rho}'_{1,2} & \hat{\rho}'_{1,3} & \cdots \\ \hat{\rho}'_{1,2}^* & 0 & 0 & \vdots \\ \hat{\rho}'_{1,3}^* & 0 & 0 & \vdots \\ \vdots & \cdots & \cdots & \ddots \end{bmatrix}, \quad (\text{I.15})$$

which has eigenvalues

$$\lambda = \frac{1}{2} \left(\hat{\rho}'_{1,1} \pm \sqrt{\hat{\rho}'_{1,1}{}^2 + 4 \sum_{n=2}^{(n_{\text{max}}+1)^2} |\hat{\rho}'_{1,n}|^2} \right), \quad (\text{I.16})$$

and all other eigenvalues are 0. However, $|\hat{\rho}'_{1,n}|^2 = O(\mu^2)$, so the only non-zero first order eigenvalue is $\lambda_1 = \hat{\rho}'_{1,1}$. Further, $\hat{\rho}'_{1,1}$ has contribution $\hat{\rho}_{1,1}^2$, which has non-zero constant contribution due to $(1 - \mu)^{n_{\text{loss}}}$. To the second order, the λ 's are

$$\{a + b\mu + c\mu^2, O(\mu^2), O(\mu^2), O(\mu^2), \dots\}. \quad (\text{I.17})$$

Therefore, after normalization of the eigenvalues, the entropy contribution due to λ_1 is

$$-\frac{a + b\mu + c_1\mu^2}{a + b\mu + d\mu^2} \log \frac{a + b\mu + c\mu^2}{a + b\mu + d\mu^2} = \frac{(d - c)\mu^2}{a \ln 2} + O(\mu^3) = O(\mu^2), \quad (\text{I.18})$$

where $d = \sum_i c_i$ is the sum of second-order coefficients of all eigenvalues. Contribution of other singular values are

$$-\frac{c_i\mu^2}{a + b\mu + d\mu^2} \log \frac{c_i\mu^2}{a + b\mu + d\mu^2} = O(-\mu^2 \log \mu). \quad (\text{I.19})$$

Therefore, regardless of the initial state, the entanglement entropy scales as $O(\mu^2 \log \mu)$. Since the total entanglement entropy is the sum of all N input modes, we obtain, for $\mu \rightarrow \beta N^\gamma / N$,

$$S_1(|\hat{\rho}\rangle\rangle) = O \left(N \left(\frac{\beta N^\gamma}{N} \right)^2 \log \left(\frac{\beta N^\gamma}{N} \right) \right) = O(N^{2\gamma-1} \log N). \quad (\text{I.20})$$

II. SUPPLEMENTARY FIGURES

Fig. 1 shows the computational time of the GPU-based implementation, and Fig. 2 shows contributions from subroutines. All experiments are performed with $N = 5$, $M = 32$, $\mu = 0.5$, $r = 0.88$ on a single A100 GPU. We see that the contribution from the tensor contraction step is minimal compared to the total simulation time thanks to the efficient custom kernel. Further, SVD takes up the majority of the simulation time, meaning that the overhead of tensor sorting, alignment, and storage is acceptable.

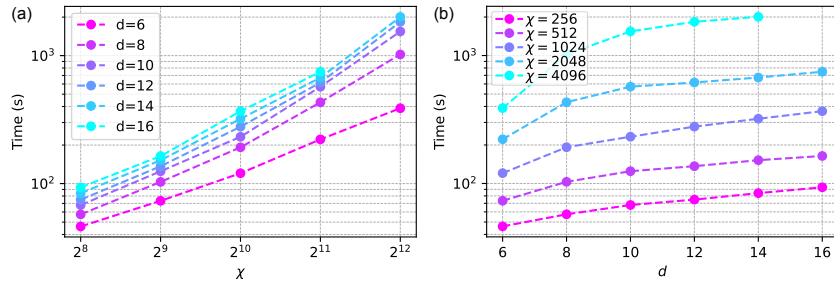


FIG. 1: Simulation time of the GPU algorithm. (a) Computational time versus bond dimension at fixed local Hilbert space sizes. (b) Computational time versus local Hilbert space sizes at fixed bond dimensions.

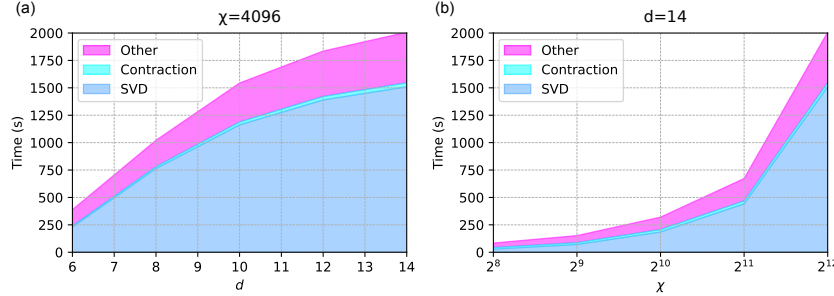


FIG. 2: Contribution to simulation time of the GPU algorithm from subroutines. (a) Bond dimension $\chi = 4096$. (b) Local Hilbert space size $d = 14$.

All CPU simulations are performed with a single node of the Bebop system with 36 cores, and GPU simulations are performed with a single Polaris GPU. A single node at the Polaris system has 4 GPUs, so a single node speed from Bebop to Polaris is even more significant. The additional higher level parallelism that allows multi-GPU and multi-node computation means that we can achieve even more significant speed up compared to the previous implementation.

[1] Changhun Oh, Kyungjoo Noh, Bill Fefferman, and Liang Jiang, “Classical simulation of lossy boson sampling using matrix product operators,” *Phys. Rev. A* **104**, 022407 (2021).